Available online at www.sciencedirect.com
ScienceDirect
Journal of the European Ceramic Society 29 (2009) 763–771
www.elsevier.com/locate/jeurceramsoc

Fracture toughness determination of $Ti_3Si(Al)C_2$ and Al_2O_3 using a single gradient notched beam (SGNB) method

Detian Wan [b], Yiwang Bao [b], Jianzhong Peng [b], Yanchun Zhou [a,*]

[a] *Shenyang National Laboratory for Materials Science, Institute of Metal Research, Chinese Academy of Sciences, 72 Wenhua Road, Shenyang 110016, PR China*
[b] *China Building Materials Academy, Beijing 100024, PR China*

Received 14 February 2008; received in revised form 26 May 2008; accepted 13 June 2008
Available online 15 August 2008

Abstract

In this work, we suggest a new and simple method named single gradient notched beam (SGNB) method for determining the fracture toughness of $Ti_3Si(Al)C_2$ and Al_2O_3 with four-point bending specimens. For the specimen with a gradient notch, a sharp natural crack will initiate and extends from the tip of the triangle under increasing load. Based on the straight through crack assumption or on the slice model, the stress intensity factor coefficient for this notched beam was derived. The fracture toughness can be calculated from the maximum load and the minimum of the stress intensity factor coefficient without knowing the crack length. To verify the feasibility and reliability of this suggested method, the SGNB method and two other conventional methods, e.g. the chevron notched beam (CNB) method and single edge notched beam (SENB) method, were performed to determine the fracture toughness of $Ti_3Si(Al)C_2$ and Al_2O_3. The measured fracture toughness values obtained from the SGNB method agreed well with those from conventional fracture toughness tests.

Keywords: Testing; Toughness; Ti_3SiAlC_2; Mechanical properties

1. Introduction

Fracture toughness K_{IC} is commonly regarded as one of the most important material properties in fracture mechanics of ceramics because it reflects the resistance to crack growth. Since K_{IC} measures the ability of a material containing a flaw to withstand an applied load, it is an important property for designing and selecting an engineering material while taking into account the inevitable presence of flaws.[1] Fracture is often caused by a propagating crack, which originates from flaws and extends when the stress intensity factor exceeds the fracture toughness. The fracture toughness of a brittle material is characterized by a critical level of the stress intensity factor near the crack tip at which a crack starts to propagate, and is assumed to be independent of flaw size, sample shape, and the stress distribution. To evaluate the fracture toughness of ceramics accurately, much attention has been paid by many material and mechanical scientists.[2–15] Generally, for test methods rely on the formation of a machined notch, the notch width should be sufficiently narrow to simulate the true crack propagation. Below a critical slot width (or notch width), the observed "K_{IC}" is a constant and equals to the plane strain fracture toughness that is obtained from specimens with sharp cracks.[2–10]

The common testing methods for determining the fracture toughness of monolithic ceramics include the single-edge notched beam (SENB),[2,3] single-edge pre-cracked beam (SEPB),[4–6] chevron-notched beam (CNB),[7–10] indentation strength (IS),[11,12] indentation fracture (IF),[11,13] and surface crack in flexure (SCF)[14,15] tests. Since the indentation crack is hard to induce in a quasi-plastic ceramic like Ti_3SiC_2, the IS, IF, and SCF methods are unsuitable for K_{IC} measurement for this kind ceramics,[16] which is a disadvantage of these three methods. Although the SEPB method may be the most valid one from theoretical consideration because this method can simulate the true crack in the testing specimen, precracked specimens are difficult to prepare in a reproducible manner, and the initial crack front often cannot be seen on the fracture surfaces after testing, making it nearly impossible to measure the crack length.[17] For the SENB method, notch preparation is critical in the determination of the plane strain fracture toughness K_{IC}.[2,3,8,18] Many

* Corresponding author. Tel.: +86 24 23971765; fax: +86 24 23891320.
E-mail address: yczhou@imr.ac.cn (Y. Zhou).

0955-2219/$ – see front matter © 2008 Elsevier Ltd. All rights reserved.
doi:10.1016/j.jeurceramsoc.2008.06.031

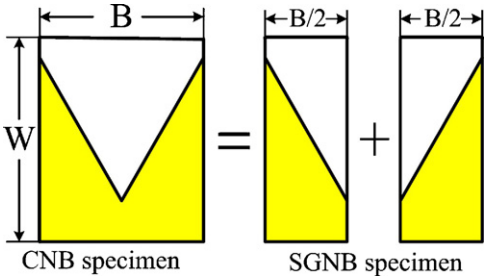

Fig. 1. Relationship between the CNB specimen and the SGNB specimen. Noting that the SGNB specimen can be considered as one half of the CNB specimen.

works have shown that the notch width should be sufficiently small (e.g. less than 66 μm for Al_2O_3)[8] when the SENB method is used; otherwise, the measured toughness increases a lot with the increment of notch width.[8,18,19] In the CNB method, the fact that a sharp crack develops at the notch tip and extends stably as the load is increased is a unique advantage for the determination of the plane strain fracture toughness.[7–10,20] Moreover, the CNB method can also be used to evaluate the high-temperature fracture toughness of ceramics.[8,21] Due to the apparent advantages, the CNB method has been widely used[7–10,20,21] and is recognized as a standard method to measure the fracture toughness of ceramic materials.[22] However, it is often difficult to make the two half-notched surfaces on the same plane, leading to the difficulty in preparing the test specimens.[23] This method is also unsuitable to evaluate the *R*-curve of a material because the initial crack growth length cannot be measured before experimental tests. Hence, the testing methods for determining the fracture toughness of ceramics mentioned above are either difficult in terms of preparing the testing specimens or in having some limitations.

To measure the fracture energies of firebricks directly, Nakayama[24] firstly suggested that the test specimen should be made with a deep triangular notch by a diamond cutting blade. It was revealed that the crack extention was stable during the testing. Recently, Bao et al.[16] have used this method to precrack a beam of ceramics for fracture toughness experiments. It was demonstrated that a sharp crack initiated from the tip of the triangle and that the crack propagation length was controllable. By looking at the fracture surfaces, we found that the crack fronts were nearly linear. These results have encouraged us to find a new method, which can determine the fracture toughness of ceramics accurately with few limitations, and for which it is easy to prepare the testing samples. Because the triangle shape in the specimen can be considered as a gradient notch, this new method for determining the fracture toughness is named as the single-gradient notched beam (SGNB) method. In addition, the SGNB specimen can be regarded as one half of the CNB specimen as shown in Fig. 1. Therefore, the SGNB method is somewhat similar to the CNB method and will have the following advantages, which will be discussed in the later section: (1) the benefits of the CNB method, (2) in situ observation of the crack propagation, (3) indication of the *R*-curve, and (4) simple preparation of the testing specimen.

In the present work, the stress intensity factor coefficient was derived based on the straight through crack assumption or the slice model. Analytical relationship to determine the fracture toughness of ceramics was obtained. Because $Ti_3Si(Al)C_2$ is a typical quasi-plastic ceramic and Al_2O_3 is a typical brittle one, these two materials were used as the testing samples and the fracture toughness values were determined using the SGNB method to represent the application of this new method. To verify the feasibility and reliability of the SGNB method, two other conventional methods, e.g. the SENB and CNB methods, were also utilized to determine the fracture toughness of $Ti_3Si(Al)C_2$ and Al_2O_3.

2. Basic principle

2.1. Stress intensity factor for a specimen with a gradient notch

A four-point bending specimen with a gradient notch is characterized by the dimensions as shown in Fig. 2: B the thickness of the sample, W the height, S_i the inner span, S_o the outer span, a_0 and a_1 notch length, and θ notch angle. The length of the crack front b at crack length is

$$b = B\left[\frac{a-a_0}{a_1-a_0}\right] = B\left[\frac{\alpha-\alpha_0}{\alpha_1-\alpha_0}\right] \quad (1)$$

where $\alpha_i = a_i/W$. The symbols are shown in Fig. 2(b).

Considering the available energy and the necessary energy for crack propagation through the rule of energy, the relationship between load P and fracture toughness K_{IC} (mode I) can be

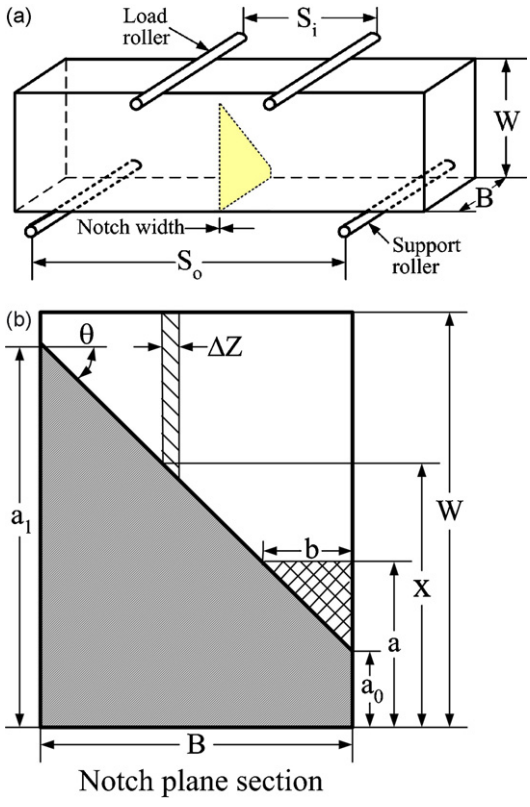

Fig. 2. (a) Four-point bending specimen with a gradient notch and (b) cross section of the gradient notch.

obtained. The available energy for the extension of crack by Δa is

$$\Delta U = \left[\frac{P^2}{2W}\right]\left(\frac{dC_{tr}}{d\alpha}\right)\Delta a \quad (2)$$

where C_{tr} is the compliance of the specimen with a triangle crack front (Fig. 2).

When the crack extends by an increment Δa, the crack area will increase by $\Delta A = b\Delta a$, and the necessary energy for crack extension is given by

$$\Delta N = G_{IC} b\,\Delta a = \left(\frac{K_{IC}^2}{E'}\right) b\,\Delta a \quad (3)$$

where $E' = E$ for plane stress, $E' = E/(1-\nu^2)$ for plane strain.

During the extension of the crack, let $\Delta N = \Delta U$, the stress intensity factor K_{IC} is obtained

$$K_{IC} = P\left[\frac{(dC_{tr}/d\alpha)E'}{2Wb}\right]^{1/2} = \frac{P}{B\sqrt{W}}\left[\frac{1}{2}\frac{dC'_{tr}}{d\alpha}\frac{\alpha_1-\alpha_0}{\alpha-\alpha_0}\right]^{1/2} \quad (4)$$

where $C'_{tr} = E'BC_{tr}$ is the dimensionless compliance, and the stress intensity factor coefficient Y^* is given by

$$Y^* = \left[\frac{1}{2}\frac{dC'_{tr}}{d\alpha}\frac{\alpha_1-\alpha_0}{\alpha-\alpha_0}\right]^{1/2} \quad (5)$$

The stress intensity factor coefficient will first decrease during the crack extension and then increases after reaching a minimum, Y^*_{min}. Maximum load P_{max} occurs at the minimum value of Y^*_{min}. Generally, because the maximum load can be determined from experiment easily, the stress intensity factor is often calculated from the maximum load P_{max} and Y^*_{min},

$$K_{IC} = \frac{P_{max}}{BW^{1/2}} Y^*_{min}. \quad (6)$$

2.2. Stress intensity factor coefficient Y^*

To calculate K_{IC} from P_{max} and Y^*_{min} using Eq. (6), the compliance function of the specimen with a gradient notch must be known. Under the assumption that the derivative of the compliance for a specimen with a gradient notch with respect to α is the same as that of a specimen with a straight through crack, the stress intensity factor coefficient Y^* can be derived. If the value of Y^* as a function of α is determined, Y^*_{min} will be obtained.

2.2.1. Y* calculated based on the straight through notch assumption

The stress intensity factor coefficient, Y^*, can be calculated based on the straight through crack assumption (STCA). For the straight notch model,[8] the stress intensity factor coefficient, Y, is

$$Y = \frac{S_o - S_i}{W} \times \frac{3\Gamma_M\sqrt{\alpha}}{2(1-\alpha)^{3/2}} \quad (7)$$

where S_o, S_i are the outer and inner span in the four point bending tests (Fig. 2), respectively,

$$\Gamma_M = 1.9887 - 1.326\alpha - \frac{[3.49 - 0.68\alpha + 1.35\alpha^2]\alpha(1-\alpha)}{(1+\alpha)^2}.$$

Thus,

$$Y^* = Y\left[\frac{\alpha_1-\alpha_0}{\alpha-\alpha_0}\right]^{1/2} = \frac{S_o - S_i}{W}\left[\frac{\alpha_1-\alpha_0}{\alpha-\alpha_0}\right]^{1/2}\frac{3\Gamma_M\sqrt{\alpha}}{2(1-\alpha)^{3/2}} \quad (8)$$

where S_o/W and S_i/W are the relative spans.

2.2.2. Y* calculated based on the Bluhm slice model

The straight through crack compliance can be used for a chevron notched specimen in a refined way using an approach offered by Bluhm.[25] Since the SGNB specimen can be considered as one-half of the chevron notched specimen, this approach can also be used for the gradient notched specimen and the stress intensity factor coefficient Y^* can be derived in a refined way as for the CNB specimen.[8] When the gradient notched specimen is loaded, a crack initiates at the tip producing a crack front of length b (Fig. 2). To estimate the compliance of the specimen with its trapezoidal crack (or notch), Bluhm divided the specimen into n slices of uniform thickness Δz, in which m slices are contained in the straight-through portion of the trapezoid and (n–m) slices in the tapered portion. The crack length of a slice in the slice model is x as shown in Fig. 2. In the straight-through notch region, the crack length is a constant, viz. $x = a$.

The compliance of a slice of thickness $\Delta z = B/n$ and crack length-to-height ratio $\xi = x/W$ is

$$C_s(\xi) = C(\xi)\left(\frac{B}{\Delta z}\right) \quad (9)$$

where $C(\xi)$ is the compliance of a straight-through crack specimen, B the specimen thickness, ξ the relative crack length.

Bluhm recognized that the compliance of the slices is affected by the interlaminar shear stresses. Accounting for this shear stresses, the slice thickness, Δz, is replaced by an effective thickness $\Delta z' = k\Delta z$.

For the portion of the specimen with a tapered crack front,

$$C_s(\xi) = C(\xi)\left(\frac{B}{\Delta z'}\right) \quad (10)$$

For the portion with a straight through crack front of length b, there are no interlaminar shear stresses and therefore $k = 1$. The thickness of a slice in this region can be expressed as $\Delta z = b/m$ and the compliance of a slice is given by

$$C_s(\alpha) = C(\alpha)\left(\frac{B}{\Delta z}\right) = C(\alpha)\left(\frac{B}{b}\right)m \quad (11)$$

The total compliance C_{tr} of the trapezoidal-crack specimen is obtained by summing the reciprocals of the compliance of the slices,

$$\frac{1}{C_{tr}} = \sum_{i=1}^{n}\left(\frac{1}{C_s}\right)_i \quad (12)$$

This equation may be expressed in partitioned form as:

$$\frac{1}{C_{tr}} = \sum_{i=1}^{m}\left[\frac{1}{C_s(\alpha)}\right]_i + \sum_{i=m+1}^{n}\left[\frac{1}{C_s(\xi)}\right]_i \tag{13}$$

The form of Eq. (13) can be changed to

$$\frac{1}{C_{tr}} = \frac{1}{C_s(\alpha)}\left(\frac{\alpha-\alpha_0}{\alpha_1-\alpha_0}\right) + \frac{k}{n}\sum_{i=m+1}^{n}\left[\frac{1}{C_s(\xi)}\right]_i \tag{14}$$

In the above equation, the single slice can be treated as a straight-through crack specimen and the compliance is obtained by integrating Eq. (7),

$$C_s(\xi) = \left(\frac{2}{E'B}\right) \times \int_0^{\xi} Y^2(\xi)\,d\xi + C_0 \tag{15}$$

and

$$C_s(\alpha) = \left(\frac{2}{E'B}\right) \int_0^{\alpha} Y^2(\xi)\,d\xi + C_0 \tag{16}$$

where C_0 is the compliance of a specimen without a notch or crack and given by,[25]

$$C_0 = \frac{1}{E'B}\left(\frac{S_o - S_i}{W}\right)^2\left[\frac{S_o + 2S_i}{4W} + \frac{(1+\nu)W}{2(S_o+S_i)}\right] \tag{17}$$

No analytical solution exists for the interlaminar shear factor k in Eq. (14). Bluhm evaluated k by comparing experimental compliance measurements with the predicted compliance and found that it depended on the notch angle θ and maximum relative depth α_1. By curve fitting, a relationship between k, α_1, and θ (in rads) was obtained,

$$k = 1 + \alpha_1^{3.12}(2.263\theta - 4.744\theta^2 + 4.699\theta^3 - 1.774\theta^4)$$

$$\text{for } 0 < \theta < 1 \tag{18a}$$

$$k = 1 + 0.444\alpha_1^{3.12} \quad \text{for } \theta \geq 1 \tag{18b}$$

The notch angle θ can be calculated from

$$\theta = \tan^{-1}\left[\frac{(\alpha_1-\alpha_0)W}{B}\right] \tag{19}$$

3. Analytical results

Based on STCA, the stress intensity factor coefficient Y^* can be calculated according to Eq. (8) for a gradient notched specimen (in four-point bending model) with $B/W = 0.75$, $S_i/W = 2.5$, $S_o/W = 7.5$, and $\nu = 0.2$. Fig. 3(a) shows Y^* as a function of α for several α_0 ($0.12 \leq \alpha_0 \leq 0.24$) and $\alpha_1 = 1$ from STCA. If the Bluhm slice model is used, C_{tr} is calculated from Eq. (13) under the same specimen and parameters. When C_{tr} is known, $C'_{tr} = E'BC_{tr}$ can be calculated, and then Y^* is derived according to Eq. (5) using $n = 500$, which is sufficient to get an exact value of Y^* similar to those in CNB method.[8] Fig. 3(b) exhibits Y^* as a function of α for several α_0 ($0.12 \leq \alpha_0 \leq 0.24$) and $\alpha_1 = 1$ from the slice model. It can be seen that for both STCA and the slice model, there is a minimum for all α_0 curves (as indicated by the arrows in Fig. 3(a) and (b)). The calculated Y^*_{min}

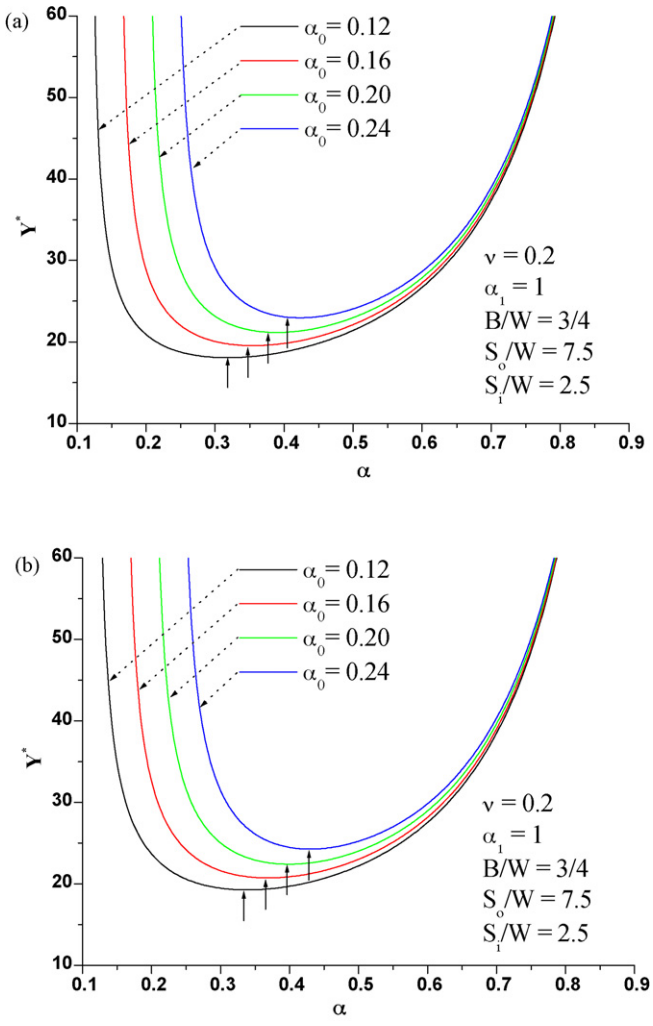

Fig. 3. Effect of the ratio of the crack length to height, α, on dimensionless parameter Y^* calculated based on the straight through crack assumption (a) and with the slice model (b) arrows indicate the minimum value of Y^*.

and the corresponding crack length to height α_{min} increase with increasing α_0. When the value of α_1 is ranged from 0.9 to 1.0, Y^*_{min} can be calculated for each condition using the same procedure mentioned above, and these results are summarized in Table 1.

The results for $B/W = 0.75$, $S_i/W = 2.5$, $S_o/W = 7.5$, $0.12 \leq \alpha_0 \leq 0.24$, $0.90 \leq \alpha_1 \leq 1.0$, and $\nu = 0.2$ are given in Table 1 as the "exact" values. By curve-fitting the "exact" data, the following two close relationships were obtained for the range of geometries consideration,

Slice model:

$$Y^*_{min} = [3.11 + 3.85\alpha_0 + 11.83\alpha_0^2]\left(\frac{S_o - S_i}{W}\right) \times \left[1 + 0.007\left(\frac{S_o S_i}{W^2}\right)^{1/2}\right]\left[\frac{\alpha_1 - \alpha_0}{1-\alpha_0}\right] \tag{20}$$

Table 1
The stress intensity factor coefficient minimum value Y_m^* determined using the slice model and using the straight through crack assumption (STCA), compared with the data calculated from the curve fitted Eqs. (20) and (21)

α_1	α_0	Y_m^*			
		Slice mode		STCA	
		Exact data	Eq. (20)	Exact data	Eq. (21)
1	0.12	19.26	19.28	18.07	18.04
	0.16	20.73	20.75	19.54	19.51
	0.20	22.41	22.43	21.17	21.15
	0.24	24.27	24.29	22.97	22.94
0.95	0.12	18.02	18.18	17.55	17.52
	0.16	19.40	19.52	18.95	18.92
	0.20	21.08	21.02	20.49	20.48
	0.24	22.74	22.69	22.20	22.18
0.90	0.12	16.89	17.09	17.01	16.98
	0.16	18.29	18.24	18.34	18.32
	0.20	19.83	19.62	19.80	19.78
	0.24	21.56	21.10	21.40	21.38

STCA:

$$Y^*_{\min} = [2.92 + 4.52\alpha_0 + 10.14\alpha_0^2]\left(\frac{S_o - S_i}{W}\right)\sqrt{\frac{\alpha_1 - \alpha_0}{1 - \alpha_0}} \quad (21)$$

Compared the $Y^*_{\min}$ value from STCA with the result given in Ref.[10], the same form of $Y^*_{\min}$ is found. This is ascribed to the fact that the CNB specimen can be considered as two parallel connected SGNB specimens and $k = 1$. The $Y^*_{\min}$ values calculated using Eqs. (20) and (21) are also presented in Table 1. For the slice model, the differences between the "exact" values and those calculated from Eq. (20) never exceed 2.1%. For STCA, the differences between the "exact" values and those calculated from Eq. (21) never exceed 0.2%. It is seen that the $Y^*_{\min}$ values calculated based on the Bluhm's slice model are slightly higher than that from STCA. The difference in all cases is less than 6.3%, and decreases with increasing α_0 and decreasing α_1.

It is noted that for the test specimens with the dimension of 3 mm × 4 mm × 36 mm or 3 mm × 4 mm × 45 mm, the loading speed ≤0.05 mm/min, and the major span/minor span of 40/20 mm or 30/10 mm (in four point bending test), are recommended for the CNB method and good results are obtained.[7–10,20–23] Moreover, the SGNB method has some intrinsic relationships with the CNB method, as pointed out in the introduction section. Hence, for the SGNB method, it is recommended that the sample dimension is 3 mm × 4 mm × 36 mm or 3 mm × 4 mm × 45 mm, the relative initial crack length α_0 and the relative length of the gradient notch at the surface α_1 are in the range of $0.12 \le \alpha_0 \le 0.24$ and $0.90 \le \alpha_1 \le 1.0$, respectively. The loading speed should be ≤0.05 mm/min in four-point bending test. To prepare the testing sample expediently, $\alpha_0 = 0.2$ and $\alpha_1 = 0.95$ and $\theta = \pi/4$, viz. $a_0 = 0.80$ mm and $a_1 = 3.80$ mm (sample height of 4 mm) is highly recommended for the SGNB method. Certainly, the bending fixture and the testing machine must be sufficiently stiff.

4. Experimental materials and procedure

Four-point bending tests are performed on $Ti_3Si(Al)C_2$ and sintered Al_2O_3. Bulk $Ti_3Si(Al)C_2$ material was fabricated by in situ hot pressing/solid–liquid reaction synthesis, as described elsewhere.[26,27] Briefly, the materials were prepared according to the following procedure. The mixed powders, Ti (99%, −300 mesh), Si (99.5%, −300 mesh), Al (99%, −200 mesh), and graphite (98%, −200 mesh) with the target compositions were milled for 15 h in a wet medium. After milling and drying, the mixtures were screened through a 60-mesh sieve and cold compacted into a disc of 50 mm in diameter in a graphite mold whose inner surface had been coated with boron nitride (BN). The green samples were then hot pressed at 30 MPa under a flowing Ar atmosphere at 1560 °C for 60 min, and subsequently annealed at 1400 °C for 30 min. For the bulk Al_2O_3 samples, Al_2O_3 powder (99%, ≤1 μm) was used as the initial material and cold compacted into a desired shape. The green compacts were then pressureless sintered at 1600 °C for 120 min, without additives.

The densities of the as-prepared materials were determined by Archimedes's method. The phase compositions were identified by X-ray diffraction (XRD) using powders from the bulk samples. The XRD data were collected by a step-scanning diffractometer with Cu Kα radiation (Rigaku D/max-2400, Tokyo, Japan). The microstructure of $Ti_3Si(Al)C_2$ and Al_2O_3 were observed in a SUPRA 35 scanning electron microscope (SEM) (LEO, Oberkochen, Germany) equipped with an energy-dispersive spectroscopy system. To expose the $Ti_3Si(Al)C_2$ grains, samples were mechanically polished up to 1200# SiC paper and etched by a HNO_3:HF:H_2O (1:1:2) solution before SEM observations.

Specimens with dimensions of 3 mm × 4 mm × 36 mm were prepared for $Ti_3Si(Al)C_2$ using an electrical-discharge machine and for Al_2O_3 by diamond-coated wheel slotting from the as-prepared bulk samples. One group of the samples is for the flexural strength tests and the other group is for the fracture toughness measurements using the SGNB and CNB method. Three-point bending tests with a crosshead speed of 0.5 mm/min were performed to measure the flexural strength of $Ti_3Si(Al)C_2$ and Al_2O_3. The Vickers hardness was tested on the polished surfaces at 9.80 N with a dwell time of 15 s. The dynamic elastic moduli of $Ti_3Si(Al)C_2$ and Al_2O_3 were measured at room temperature in a RFDA-HTVP1750-C testing machine (IMCE, Diepenbeek, Belgium).[26] The samples used were rectangular bars of 3 mm × 15 mm × 40 mm for $Ti_3Si(Al)C_2$ and 7 mm × 45 mm × 95 mm for Al_2O_3, respectively.

The gradient notches were introduced by diamond-coated wheel slotting. To study the effect of notch width on the fracture toughness, four types of blade with different thicknesses of 0.054, 0.117, 0.169, and 0.365 mm, were used to introduce the gradient notches. After that, the true notch width was measured by optical microscope (OM). Four-point bending tests (major span $S_o = 30$ mm, minor span $S_i = 10$ mm) with a crosshead speed of 0.05 mm/min were conducted for fracture toughness measurements. The fractured surface was examined by means of SEM and OM. In each condition, 3–5 specimens were tested to ensure

the reproducibility. The force was recorded as a function of testing time during loading. The fracture toughness measured with the four-point bending tests using SGNB specimens was calculated using Eq. (6). The stress intensity factor coefficient Y^*_{min} for the SGNB method was given in Eq. (20) for slice model and Eq. (21) for STCA.

To verify the feasibility and reliability of the SGNB method, two other conventional methods, viz. the SENB and CNB methods, were used to measure the toughness of $Ti_3Si(Al)C_2$ and Al_2O_3 and compared with the results from the SGNB method. The samples used were rectangular bars of 3 mm × 4 mm × 36 mm in size ($0.12 \le \alpha_0 \le 0.24$ and $0.90 \le \alpha_1 \le 1.0$) for CNB method and 4 mm × 8 mm × 36 mm (notch length about 4 mm) for SENB method. The notch width was about 141 and 150 μm for CNB and SENB method, respectively. The same crosshead speed of 0.05 mm/min was used.

5. Results and discussion

XRD analysis revealed that no impurities like TiC or $TiSi_2$ were detected in $Ti_3Si(Al)C_2$ and no impurities were found in Al_2O_3 (not shown here). Fig. 4(a) shows the etched surface of $Ti_3Si(Al)C_2$ and Fig. 4(b) shows the fracture surface of Al_2O_3. The large elongated $Ti_3Si(Al)C_2$ grains show layered characteristics and their longitudinal edges are parallel to (0 0 0 1) planes of Ti_3SiC_2.[28] It can be found that the grain size of Al_2O_3 is 2–5 μm, and the grain length and grain width of the $Ti_3Si(Al)C_2$ samples are 16.4 ± 7.5 and 5.0 ± 3.4 μm, respectively. The physical and mechanical properties of $Ti_3Si(Al)C_2$ and Al_2O_3 samples are summarized in Table 2.

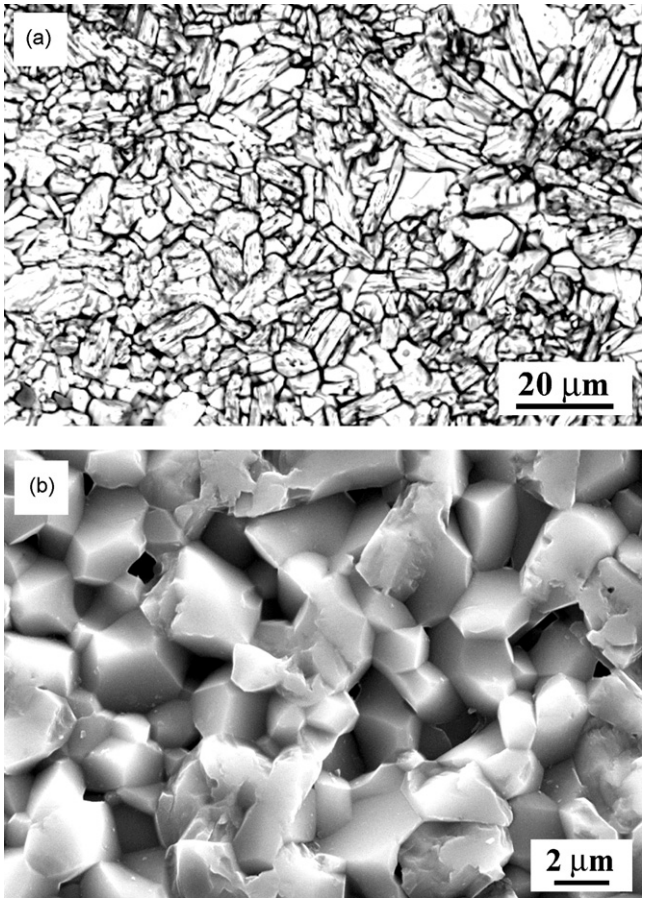

Fig. 4. SEM of the etched surface of $Ti_3Si(Al)C_2$ (a) and fracture surface of Al_2O_3 (b).

Table 2
Physical and mechanical properties of $Ti_3Si(Al)C_2$ and Al_2O_3

Properties	$Ti_3Si(Al)C_2$	Al_2O_3
Density (g/cm^3)	4.475 (98.9%)	3.823 (96.1%)
Grain size (μm)	16.4 ± 7.5 (GL) 5.0 ± 3.4 (GW)	2–5
Elastic modulus (GPa)	336	373
Vicker hardness (GPa)	4.15 ± 0.17	14.21 ± 0.54
Flexural strength (MPa)	458.8 ± 23.4	307.1 ± 6.2

GL: grain length, GW: grain width.

In our work, the load vs. testing time record for the specimens with the notch width below 250 μm exhibits the expected non-linearity up to maximum load, which demonstrate that the crack propagation is stable. Fig. 5 displays typical load vs. testing time records for $Ti_3Si(Al)C_2$ and Al_2O_3 (the notch width is below 200 μm). In addition, the magnified figure of the load vs. testing time near the fracture point for Al_2O_3 is also shown in Fig. 5. The crack propagation is generally smooth and continuous except for an occasional discontinuity resulting in a "pop in" step, which is very similar to the results of Nakayama[24]. These results demonstrate that the crack propagation is stable. Fig. 6 represents the measured fracture toughness of $Ti_3Si(Al)C_2$ and Al_2O_3 as a function of the true notch width with STCA and slice model. The fracture toughness data calculated with STCA are very close to those obtained with slice model. The maximum difference between the data from STCA and those from the slice model never exceeds 3%. It can also be seen that with increasing notch width, the fracture toughness increases from 6.20 ± 0.12 MPa m$^{1/2}$ to 7.57 ± 0.26 MPa m$^{1/2}$ for $Ti_3Si(Al)C_2$, and from 3.99 ± 0.26 MPa m$^{1/2}$ to 4.42 ± 0.26 MPa m$^{1/2}$ for Al_2O_3. This phenomenon has been found in other testing

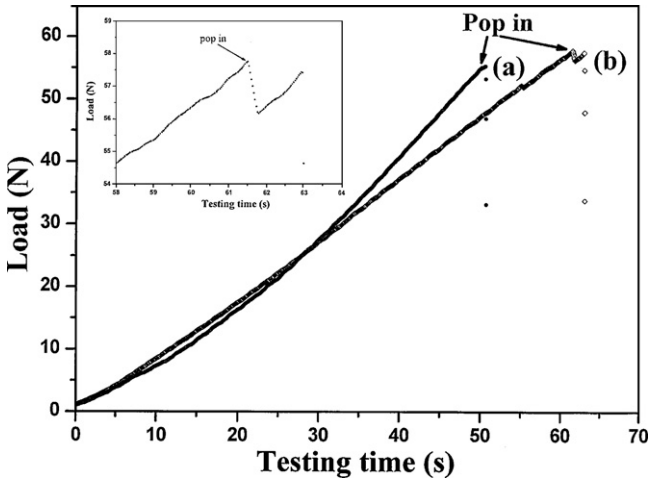

Fig. 5. Typical curve of the load as a function of testing time for $Ti_3Si(Al)C_2$ (a) and Al_2O_3 (b) with the notch width of 141 μm. The embedded figure is a magnified image for Al_2O_3 from (b) near the fracture point.

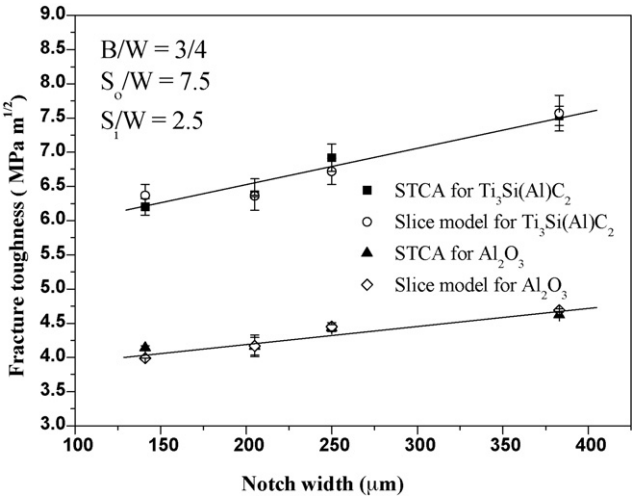

Fig. 6. Effect of notch width on K_{IC} for $Ti_3Si(Al)C_2$ and Al_2O_3 with a straight through crack assumption (STCA) and slice model.

methods like SENB[8,16,18] and CNB[18,23], which is ascribed to the effect of root radius.[29] When the notch width is $\leq$200 μm, the measured toughness of $Ti_3Si(Al)C_2$ and Al_2O_3 can be considered as a constant and a valid fracture toughness value. Fig. 7 shows a typical fractured surface of the SGNB specimen of $Ti_3Si(Al)C_2$ after bending test, which demonstrates that a successful gradient notch was introduced.

To verify the feasibility and reliability of the SGNB method, the SENB and CNB methods were also utilized to determine the fracture toughness of the same materials. Table 3 compares the

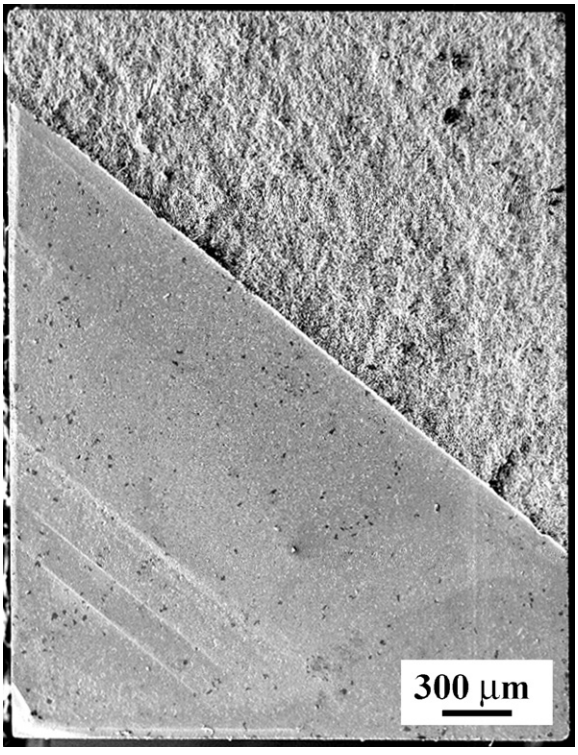

Fig. 7. Typical microphotograph of fractured surface of the SGNB specimen of Ti_3SiAlC_2.

Table 3
Measured fracture toughness of $Ti_3Si(Al)C_2$ and Al_2O_3 using the SENB, CNB, and SGNB methods

Testing method	Notch width (μm)	Fracture toughness (MPa $m^{1/2}$)	
		$Ti_3Si(Al)C_2$	Al_2O_3
SENB	150	6.80 ± 0.17	–
CNB	141	6.45 ± 0.09	4.12 ± 0.09
SGNB	141	6.20 ± 0.12	3.99 ± 0.26

measured fracture toughness of $Ti_3Si(Al)C_2$ and Al_2O_3 using the SGNB, CNB, and SENB methods. Using the CNB method at the parameters of $0.12 \leq \alpha_0 \leq 0.24$ and $0.90 \leq \alpha_1 \leq 1.0$ (notch width about 141 μm), the measured fracture toughness for $Ti_3Si(Al)C_2$ and Al_2O_3 are 6.45 ± 0.09 MPa $m^{1/2}$ and 4.12 ± 0.09 MPa $m^{1/2}$, respectively. Using the SENB method (notch width about 150 μm), the fracture toughness of $Ti_3Si(Al)C_2$ is determined to be 6.80 ± 0.17 MPa $m^{1/2}$, which is close to the measured fracture toughness from SGNB and CNB methods. The SGNB results shown in Fig. 6 are in good agreement with CNB outcomes for both materials. These results suggest the critical notch width for $Ti_3Si(Al)C_2$ and Al_2O_3 is 200 μm. Therefore, the agreement between the K_{IC} values obtained from SGNB method and those from CNB method for the testing samples with the same notch width, as well as the same Y^*_{min} calculated from STCA, demonstrates that the SGNB method is a useful and feasible method for fracture toughness determination of ceramics.

Because the specimens with a gradient notch could be used to precrack the specimen and the crack propagation can be in situ observed,[16] specimens with different crack lengths can be prepared easily. Under such a condition, the SGNB method must be available to evaluate the *R*-curve of a material. The SGNB method may cover all the advantages of CNB method[7–10,20]: (1) A sharp natural crack is produced under increasing load, (2) The test load increases nonlinearly up to a maximum load associated with stable crack extension, (3) K_{IC} is calculated from P_{max} and Y^*_{min} without crack length measurement. In addition, because a compressive load is applied on the gradient notched bend specimen to evaluate the fracture toughness of ceramics (Fig. 2), an important consideration is for high-temperature fracture toughness determination. More work is in progress to throw light on these aspects.

6. Conclusions

A new and simple method named single gradient-notched beam (SGNB) method was introduced to determine the fracture toughness of ceramics. From the analytical studies and experimental results on $Ti_3Si(Al)C_2$ and Al_2O_3, the following conclusions can be drawn:

1. A sharp natural crack is initiated at the tip of the gradient notch, and it extends under increasing load. The crack propagation is generally smooth and continuous except for an occasional discontinuity resulting in a "pop in" step. Fracture toughness K_{IC} can be calculated from the maximum load and Y^*_{min} under the assumption that the derivative of the com-

pliance for a specimen with a gradient notch with respect to α is the same as that of a specimen with a straight through crack.

2. For the SGNB method, it is recommended that the sample dimension is 3 mm × 4 mm × 36 mm or 3 mm × 4 mm × 45 mm, the initial crack length α_0 and the length of the gradient notch at the surface are in the range of $0.12 \le \alpha_0 \le 0.24$ and $0.90 \le \alpha_1 \le 1.0$, respectively. To prepare the testing sample expediently, $\alpha_0 = 0.2$ and $\alpha_1 \le 0.95$ and $\theta = \pi/4$ is highly recommended.
3. The measured fracture toughness using the SGNB method seems to decrease with decreasing slot width. The critical notch width for $Ti_3Si(Al)C_2$ and Al_2O_3 is 200 μm. With the narrowest notch width (141 μm), the fracture toughness is $6.20 \pm 0.12\,MPa\,m^{1/2}$ for $Ti_3Si(Al)C_2$, and $3.99 \pm 0.26\,MPa\,m^{1/2}$ for Al_2O_3. The agreement between the K_{IC} values obtained from the SGNB method and those from the CNB method for the same notch width samples, as well as the same Y^*_{min} calculated from STCA, demonstrates that the SGNB method can be used for fracture toughness determination of ceramics.

Acknowledgements

This work was supported by the National Outstanding Young Scientist Foundation (No. 59925208 for Y.C. Zhou, No. 50125204 for Y.W. Bao), Natural Sciences Foundation of China under Grant Nos. 50232040, 50302011, 90403027, '863' project, "Hundred talent-plan", High-tech Bureau of the Chinese Academy of Sciences, and French Atomic Energy Commission.

Appendix A

a	crack length
Δa	crack extension
a_0	initial crack length (distance from the tip of gradient notch to tensile surface)
a_1	length of the gradient notch at the surface
b	length of crack front
B	specimen thickness
C	compliance (load line displacement divided by load)
C_s	compliance of a slice in Bluhm's model
C_{tr}	compliance of a specimen with a triangle crack front
C'_{tr}	$E'BC_{tr}$
C'	$E'BC$
E	Yong's modulus
E'	E for plane stress, $=E/(1-\nu^2)$ for plane strain
G_{IC}	critical crack extension for plane strain
k	shear transfer coefficient
K_I	model I stress intensity factor
K_{IC}	plane strain facture toughness (model I)
ΔN	necessary energy for crack extension by Δa
P	load
P_{max}	maximum load
S_i	minor load roller span (or inner span)
S_o	major load roller span (or outer span)
ΔU	available energy for the extension of crack by Δa
W	specimen height
x	crack length of a slice in Bluhm's model
Y	stress intensity factor coefficient for a straight through crack
Y^*	stress intensity factor coefficient for a trapezoidal crack
Y^*_{min}	minimum of Y^*
Δz	thickness of a slice in Bluhm's model

Greek letters

α_i	a_i/W
α_{min}	the value of α corresponding to Y^*_{min}
ζ	x/W
θ	angle of the gradient notch (in rads) (see Fig. 2)
ν	Poisson's ratio

References

1. Askeland, D. R. and Phulé, P. P., *The Science and Engineering of Materials, part 1*. Fourth ed. Thomson Learning, 2004, pp. 264–268.
2. Simpson, L. A., Hsu, T. R. and Merrett, G., Application of single-edge notched beam to fracture toughness testing of ceramics. *J. Test. Eval.*, 1974, **2**, 503–509.
3. Li, S. X., Sun, L. Z., Li, H., Li, J. B. and Wang, Z. G., Stress carrying capability and interface fracture toughness in SiC/6061 Al model materials. *J. Mater. Sci. Lett.*, 1997, **16**, 863–869.
4. ASTM C 1421-99, *Standard Test Methods for Determination of Fracture Toughness of Advanced Ceramics at Ambient Temperature, Annual Book of Standards*. ASTM, West Conshohocken, PA, 1999, vol. 15.01.
5. Nosc, T. and Fuji, T., Evaluation of fracture toughness of ceramic materials by a single-precracked-beam method. *J. Am. Ceram. Soc.*, 1988, **71**, 328–333.
6. Srawley, J. E., Wide range stress intensity factor expression for ASTM E 399 standard fracture toughness specimens. *Int. J. Fract.*, 1976, **12**, 475–476.
7. Sung, J. and Nicholson, P. S., Valid K_{IC} determination via in-test subcritical precracking of chevron-notched bend bars. *J. Am. Ceram. Soc.*, 1989, **72**, 1033–1036.
8. Munz, D. R., Bubsey, T. and Shannon Jr., J. L., Fracture toughness determination of Al_2O_3 using four-point-bend specimens with straight-through and chevron notches. *J. Am. Ceram. Soc.*, 1981, **63**, 300–305.
9. Munz, D., Bubsey, R. T. and Shannon Jr., J. L., Performance of chevron-notch short bar specimen in determining the fracture toughness of silicon nitride and aluminum oxide. *J. Test. Eval.*, 1980, **8**, 103–107.
10. Munz, D., Shannon Jr., J. L. and Bubsey, R. T., Fracture toughness calculation from maximum load in four point bend tests of chevron notch specimens. *Int. J. Fract.*, 1980, **16**, R137–R141.
11. Quinn, G. D., Salem, J., Bar-on, I., Cho, K., Foley, M. and Fang, H., Fracture toughness of advanced ceramics at room temperature. *J. Res. Natl. Inst. Stand. Technol.*, 1992, **97**, 579–607.
12. Chantikul, P., Anstis, G. R., Lawn, B. R. and Marshall, D. B., A critical evaluation of indentation technique for measuring fracture toughness: II, strength method. *J. Am. Ceram. Soc.*, 1981, **64**, 539–543.
13. Anstis, G. R., Chantikul, P. B., Lawn, R. and Marshall, D. B., A critical evaluation of indentation technique for measuring fracture toughness: I, direct crack measurements. *J. Am. Ceram. Soc.*, 1981, **64**, 533–538.
14. Dransmann, G., Steinbrech, R., Pajares, A., Guiberteau, F., Dominguez-Rodriguez, A. and Heuer, A., Indentation studies on Y_2O_3-stabilized ZrO_2: II, toughness determination from stable growth of indentation-induced cracks. *J. Am. Ceram. Soc.*, 1994, **77**, 1194–1201.
15. Quinn, G. D., Gettings, R. J. and Kűbler, J. J., Fracture toughness by surface crack in flexure (SCF) method: results of the VAMAS robin. *Ceram. Eng. Sci. Proc.*, 1994, **15**, 846–855.
16. Bao, Y. W. and Zhou, Y. C., A new method for precracking beam for fracture toughness experiments. *J. Am. Ceram. Soc.*, 2006, **89**, 1118–1121.

17. Samuel, D. C., William, R. B. and James, R. V., Fracture toughness of TiB_2 and B_4C using the single-edge precracked beam, indentation strength, chevron notched beam, indentation strength methods. *J. Am. Ceram. Soc.*, 1995, **78**, 2187–2192.
18. Bao, Y. W. and Zhou, Y. C., Effect of sample size and testing temperature on the fracture toughness of Ti_3SiC_2. *Mater. Res. Innov.*, 2005, **9**, 41–42.
19. Mukhopadhyay, A. K., Datta, S. K. and Chakraborty, D., Fracture toughness of structural ceramics. *Ceram. Int.*, 1999, **25**, 447–454.
20. Munz, D., Bubsey, R. T. and Srawley, J. E., Compliance and stress intensity coefficients for short bar specimens with chevron notches useful for fracture toughness testing of ceramics. *Int. J. Fract.*, 1980, **16**, 359–374.
21. Mizuno, M. and Okuda, H., VAMAS round robin on fracture toughness of silicon nitride. *J. Am. Ceram. Soc.*, 1995, **78**, 1793–1801.
22. ISO 24370, *Fine Ceramics (Advanced Ceramics, Advanced Technical Ceramics)—Test Method for Fracture Toughness of Monolithic Ceramics at Room Temperature by Chevron Notched Beam (CNB) Method*. International Organization for Standards, Geneva, 2005.
23. Wan, D. T., Meng, F. L., Zhou, Y. C., Bao, Y. W. and Chen, J. X., Effect of grain size, notch width, testing temperature on the fracture toughness of $Ti_3Si(Al)C_2$ and Ti_3AlC_2 using the chevron-notched beam (CNB) method. *J. Eur. Ceram. Soc.*, 2008, **28**, 663–669.
24. Nakayama, J., Direct measurement of fracture energies of brittle heterogeneous materials. *J. Am. Ceram. Soc.*, 1965, **48**, 583–587.
25. Bluhm, J. I., Slice synthesis of a three dimensional 'work of fracture' specimen-for brittle materials testing. *Eng. Fract. Mech.*, 1975, **7**, 593–604.
26. Zhou, Y. C., Wan, D. T., Bao, Y. W. and Wang, J. Y., In-situ processing and high-temperature properties $Ti_3Si(Al)C_2$/SiC composites. *Int. J. Appl. Ceram. Soc.*, 2006, **3**, 47–54.
27. Wan, D. T., Zhou, Y. C., Bao, Y. W. and Yan, C. K., In-situ reaction synthesis and characterization of $Ti_3Si(Al)C_2$/SiC composites. *Ceram. Int.*, 2006, **32**, 883–890.
28. Zhou, Y. C., Sun, Z. M. and Yu, B. H., Microstructure of Ti_3SiC_2 prepared by the in-situ hot processing/solid–liquid reaction process. *Z. Met.*, 2000, **91**, 937–941.
29. Awaji, H. and Sakaida, Y., V-notch technique for single-edge notched beam and chevron notch methods. *J. Am. Ceram. Soc.*, 1990, **73**, 3522–3523.